

# A Solar Irradiance Cross-Calibration Method Enabling Climate Studies Requiring 0.2% Radiometric Accuracies

Paul Smith, Ginger Drake, Joey Espejo, Karl Heuerman, and Greg Kopp  
Laboratory for Atmospheric and Space Physics  
1234 Innovation Drive  
Boulder, CO 80303 USA

**Abstract-** The 2007 NRC Decadal Survey's CLARREO mission requires shortwave radiometric accuracy and SI-traceability to better than 0.2% for Earth climate studies on decadal time scales. These accuracies, being nearly ten times better than current on-orbit capabilities, will establish benchmark measurements of solar radiation scattered by the Earth, provide reference calibrations for other on-orbit instruments, and initiate a climate data record to be used for future policy decisions. The methods described here promise a solution enabling such a high accuracy level via on-orbit end-to-end calibration of a hyperspectral imager using measurements of solar irradiances, which are known to better radiometric accuracies than any other calibration sources available on-orbit in the 350 – 2300 nm spectral region.

Cross-calibrating the hyperspectral imager with solar irradiances requires highly accurate attenuation methods, which are investigated in the work described here. The required attenuation between viewing solar and Earth radiances is approximately 5 orders of magnitude. Three methods are demonstrated to collectively provide this level of attenuation: decreasing optical entrance aperture size, shortening detector integration times, and inserting attenuating filters.

Apertures are demonstrated to provide 3 orders of magnitude of attenuation by switching from a 20 mm aperture when observing the Earth to a 0.5 mm diameter aperture when observing the Sun. The aperture geometric areas are calibrated by NIST, and provide the expected attenuations with 0.1% uncertainties. Integration times from electronically shuttered focal plane arrays provide attenuations of 2 orders of magnitude. The accuracy across this attenuation range is shown to be approximately 0.04%, measured by a NIST-calibrated silicon trap detector. Filters achieve 1 order of magnitude attenuation, limited by on-orbit calibrations via lunar radiance observations, a technique that has been demonstrated in the lab to 0.06% uncertainty across the visible spectral range (450 – 700 nm).

The work described here promises a solar cross-calibration approach to achieving the CLARREO mission requirements for shortwave radiometry, making it a viable option for long-term space-based climate studies.

## I. INTRODUCTION

A key component in climate studies is the balance between the Earth's incoming and outgoing radiative energy. While the incoming Sun's energy can be measured to better than 0.1% accuracy [1,2], similar measurements of the Earth's outgoing radiative energy are only known to around 2% [3-7],

limited by traditional methods of pre-launch calibrations [8-9], onboard calibration systems [6,10], or vicarious calibrations [3,11,12]. The need for even more highly accurate measurements of the Earth's radiative energy is addressed by the Committee on Earth Science and Applications from Space in the 2007 NRC Decadal Survey's recommended CLARREO mission [13], which has since refined the required accuracy to less than 0.2% ( $k=1$ ). The central objective of such an accurate long-term measurement is to provide an SI-traceable benchmark of the Earth's energy budget. Once established, CLARREO can cross-calibrate other on-orbit instruments to spatially and temporally increase accuracy of the climate record, develop operational climate forecast models, and provide a framework for future climate policy decisions.

The proposed CLARREO hyperspectral imager achieves a tenfold improvement in accuracies of an Earth-viewing instrument by transferring the expected 0.1% TSIS (Total Solar Irradiance Sensor) accuracy of solar-viewing instruments in the 350-2300 nm spectral region to an outgoing Earth energy measurement, giving the added benefit of removing a common-mode uncertainty in the relationship between incident and reflected solar radiation. To accomplish the cross-calibration via direct solar viewing, the imager utilizes three methods to collectively achieve the required five orders of magnitude of attenuation: decreasing optical entrance aperture area, shortening detector integration time, and inserting attenuating filters.

With thorough understandings of the attenuation methods and their uncertainties, complete end-to-end on-orbit calibration of the instrument is achievable using solar spectral irradiances. A laboratory quantification of each attenuation technique and their uncertainties is described here.

## II. EXPERIMENTAL SETUP

Demonstrating the proposed attenuation methods nominally requires a highly stable light source with the uniformity, irradiance, and spectrum of the Sun in orbit; unfortunately, no such broadband light source exists with the needed stability levels. Instead, a laser that can apply typical solar power levels is used. Gaussian beam expansion provides the required spatial uniformity over the instrument aperture sizes used, and

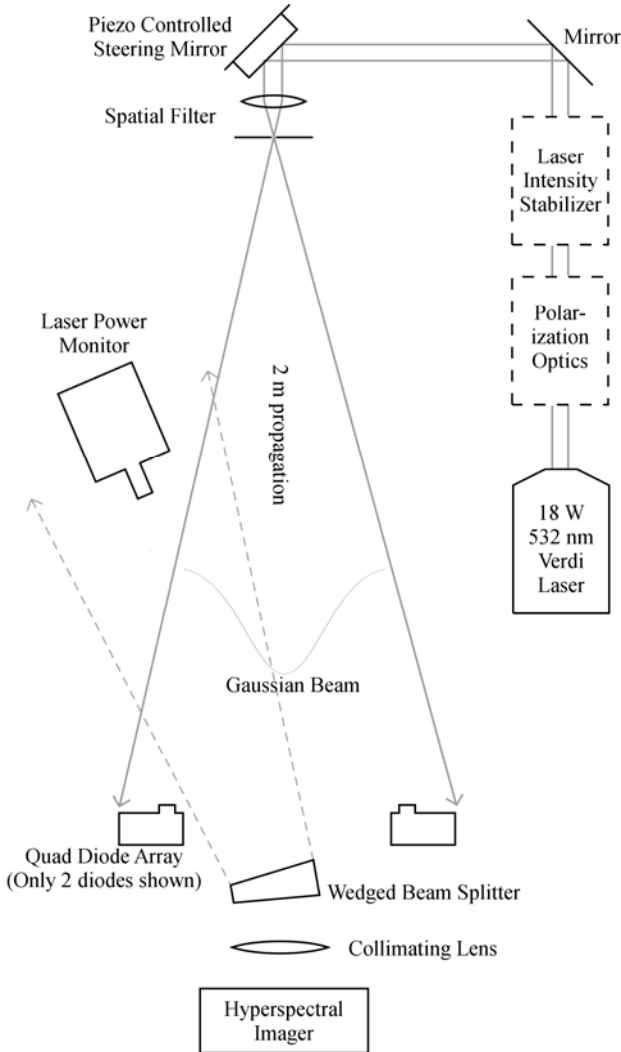


Fig. 1. Laboratory setup for testing attenuation methods. Gaussian beam expansion provides beam uniformity from a stabilized, high-power laser.

intensity control provides the needed temporal stabilities. A schematic of the setup is shown in Fig. 1.

A 532 nm, 18 W Verdi laser is near the solar peak wavelength and has sufficient power to achieve the required  $2 \text{ mW/cm}^2/\text{nm}$  typical spectral irradiance levels after power loss due to spatial filtering and beam expansion from 2 m propagation. A 15.3 mm focal length lens followed by a  $5 \mu\text{m}$  high-power pinhole spatially filters the beam for uniformity and provides  $\sim 130$  times magnification so that the beam incident on the entrance aperture of the hyperspectral imager is approximately Gaussian with a  $1/e^2$  diameter of 290 mm for uniform illumination across the much smaller aperture.

With such high magnification, even small perturbations in the input polarization and beam shaping optics due to temperature, humidity, or air current fluctuations can have large effects in the stability and positioning of the expanded Gaussian beam. In addition to mechanically stabilized optical mounts, three active methods maintain beam spatial and temporal stability. 1) Quad diode positioning feedback

sensors near the entrance aperture of the hyperspectral imager control a piezo fast steering mirror located 3 cm before the spatial filter to maintain positional beam stability. With this 5 Hz closed loop stabilization, beam motion standard deviation is  $377 \mu\text{m}$  in the vertical direction and  $350 \mu\text{m}$  in the horizontal direction over a 51 hour test. 2) A laser power controller monitors the laser beam before the spatial filter and adjusts a variable attenuator to compensate for intensity fluctuations at  $\sim 1 \text{ kHz}$ . 3) A wedged beam splitter directly in front of the hyperspectral imager input aperture monitors the center 2 mm of the beam input to the imager using a trap detector having linear response calibrated over 7 orders of magnitude of input power with uncertainties  $\leq 120 \text{ ppm}$  over the ranges used. When utilizing all three of these methods, the power instability is measured to be 120 ppm over 5 minutes and 240 ppm over 15 hours.

A 2 m focal length lens in front of the imager's entrance aperture collimates the diverging light of the expanding Gaussian beam to simulate a uniform incident solar beam. Beam uniformity is intermittently verified by placing a CCD array at the input aperture location to directly characterize the incident beam. The non-uniform gain of the CCD sensor is measured by placing it in the center of a very uniform field, generated with a  $2 \mu\text{m}$  pinhole spatial filter, which increases the  $1/e^2$  diameter of the Gaussian beam to over 1 m.

Although the solar attenuation methods applied are applicable to many instruments, they are demonstrated here using a hyperspectral imager. This imager consists of a three mirror anastigmat that focuses the incident beam onto a  $70 \mu\text{m}$  slit followed by a grating-based Offner spectrometer that disperses the beam and focuses the spatial/spectral image onto a focal plane array [14].

### III. APERTURE ATTENUATION

Three orders of magnitude of attenuation are achieved by changing from a 20 mm diameter input aperture when observing the Earth to a 0.5 mm diameter input aperture when observing the Sun. Intermediate sized apertures provide redundancy and linearity diagnostics.

NIST calibrates the aperture areas by placing the apertures on a precision rotation stage and measuring the linear distance from the center of the aperture to the diamond turned knife edge under a microscope at  $5^\circ$  increments [15]. Each aperture is measured 5 times, and the resulting measurements are fit to a circle to calculate geometric area and deviations. The final area uncertainty estimation includes standard deviation in the repeated measurements, thermal expansion uncertainties, systematic uncertainties in the stage motion and aperture edge imaging systems, and deviations from circularity. The resulting areas and uncertainties from the primary three

TABLE I  
NIST-MEASURED APERTURE AREAS AND UNCERTAINTIES

Aperture Diameter (mm)	Aperture Area ( $\text{mm}^2$ )	Area Uncertainty (ppm) ( $k=1$ )
19.9862	313.72454	17
7.9732	49.9290	25
0.51542	0.20865	317

apertures are shown in Table I.

The test facility verifies that the incident beam attenuations are proportional to the aperture areas. This relative power ratio has the benefit of being a simpler measurement than two corresponding absolute measurements. Test apertures are sequentially placed in the center of the expanded uniform Gaussian beam, schematically shown in Fig. 2, as the incident light is monitored at the output of the hyperspectral imager with a large area photodiode (Hamamatsu S6337-01) verified to be linear across the range used to 66 ppm against the NIST calibrated trap detector. Knowledge of the common mode imager component reflectivities is unnecessary in this relative measurement. Type A measurement noise after averaging 100 readings is 12 ppm over 5 minutes. The slit is removed for the power ratio measurement to help simplify possible alignment errors and alleviate mismatched scattering between different apertures, but will be repeated with the full imager setup.

An irradiance non-uniformity correction accounts for the average Gaussian beam intensity across the 0.5 mm aperture being higher than that across the 20 mm aperture, as shown schematically in Fig. 2. The actual irradiance at the input aperture location is measured by a CCD camera mounted at the aperture position. One such CCD image, corrected for dark noise and gain non-uniformities, is shown in Fig. 3a. Since the irradiance ratio between the 0.5 mm aperture and the 20 mm aperture varies across the Gaussian field, the CCD image is used to calculate the power ratio at every pixel, seen in Fig. 3b. The exact location of the center of the Gaussian field is estimated to be within 3 mm of the center of the CCD image. The non-uniformity correction is thus the mean of the power ratios within the center 9 mm<sup>2</sup> area, and the uncertainty in the correction is their standard deviation.

The results of the power ratio measurements using 20, 8, and 0.5 mm diameter apertures are shown in Table II. Switching from the 20 mm to the 8 mm aperture gives a non-uniformity corrected power ratio of 6.2843 with a non-uniformity correction uncertainty conservatively estimated at 200 ppm. Switching from the 8 mm to the 0.5 mm aperture provides a non-uniformity corrected power ratio of 239.193 with 673 ppm uncertainty, nearly all of which is due to the field non-uniformity correction uncertainty. The measured power ratio

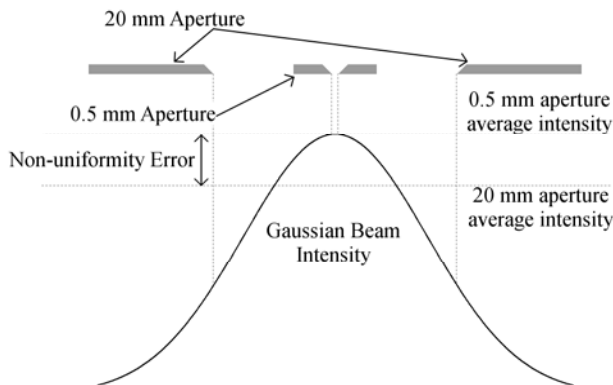


Fig. 2. Spatial beam variations causing differences between irradiances measured by each aperture are corrected by direct CCD images of the beam. (Gaussian beam variations shown are exaggerated)

TABLE II

POWER RATIO MEASUREMENTS AND UNCERTAINTIES

Aperture Ratio	NIST Area Ratio $\pm$ Uncertainty (k=1)	Power Ratio $\pm$ Uncertainty (k=1)
20/8	6.2834 $\pm$ 31 ppm	6.2843 $\pm$ 200 ppm
8/0.5	239.2954 $\pm$ 317 ppm	239.1930 $\pm$ 673 ppm

differs from the area ratio by 143 ppm and the 20 to 8 mm case and 428 ppm in the 8 to 0.5 mm case. Both these cases are within the measurement uncertainties. Combined, the total power attenuation from the 20 mm aperture to the 0.5 mm aperture is  $10^{-3.2}$  with an uncertainty of 0.07%.

#### IV. INTEGRATION TIME ATTENUATION

The second method of achieving the necessary 5 orders of magnitude of total attenuation is reducing the electronic shuttering time of the sensor, which can achieve at least 2 orders of magnitude using high speed focal plane arrays (FPAs). The laboratory demonstration sensor used here is the 12-bit Photon Focus MV1-1312-160 CMOS FPA with electronic global shuttering capabilities, necessary when measuring precise attenuations with rapid exposure times under constant illumination. The total exposure time range of the sensor is 0.01 to 420 ms, sufficient to provide 4.6 orders of magnitude of attenuation if the response is linear across the entire range. Attenuations achieved by integration time reduction have so far been tested for linearity across 2 orders of magnitude.

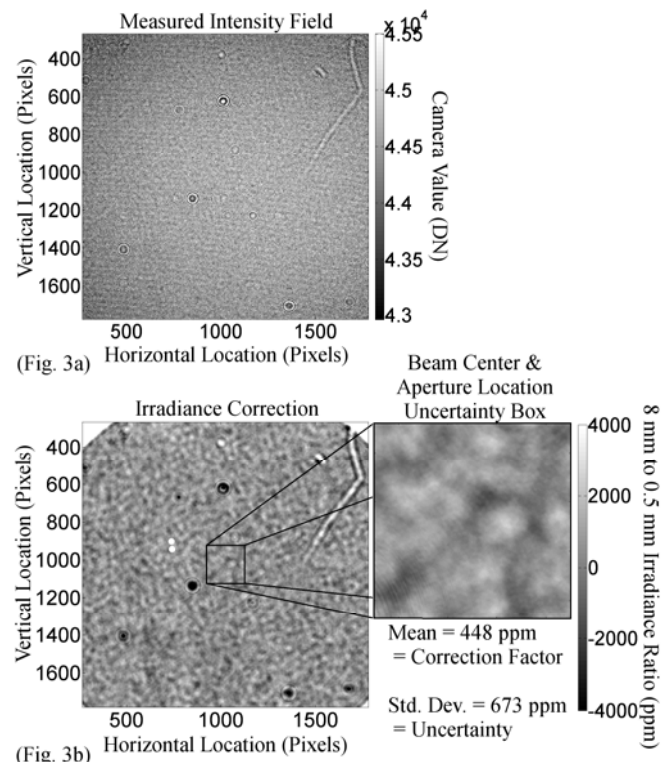


(Fig. 3a)

(Fig. 3b)

Fig. 3a. Beam intensity is measured at input aperture location to correct for spatial variations between apertures. One pixel width is 15  $\mu$ m.

Fig. 3b. Computed irradiance corrections. Uncertainty in beam center and aperture location create uncertainties in non-uniformity correction factor.

The setup for measuring the integration time attenuation is the same as in Fig. 1 with the hyperspectral imager replaced by the CMOS sensor in the Gaussian beam directly behind the wedged beam splitter. The NIST calibrated trap detector monitors the incident beam intensity, which is increased as the CMOS integration time is reduced to avoid FPA non-linearity effects. With the CMOS response thus held constant, the integration time ratio and power ratio vary inversely, providing a verification of the integration time attenuation method. Similarly to the aperture attenuation method, this measurement is relative, pinned to the ratio of the laser power measured by the trap detector that NIST calibrated over 7 orders of magnitude.

The integration time attenuation measurement uncertainty is determined by the variation in repeated measurements, giving 360 ppm for 50 measurements. The slope of the linearity curve increases at lower signal levels, indicating slight nonlinearities in the FPA sensor gain. The gain nonlinearity has been measured via comparisons to the NIST calibrated trap detector and is compensated during post processing. Residuals from linearity with the CMOS sensor response held at 2250 DN (digital number) while beam power is varied are plotted as a percentage of measured power in Fig. 4, showing a standard deviation of 302 ppm. As the signal level is reduced, both the uncertainty in the measurement and the linearity error increase, but above 1000 DN the uncertainty can be maintained to <0.1% with nonlinearities contributing <0.06%.

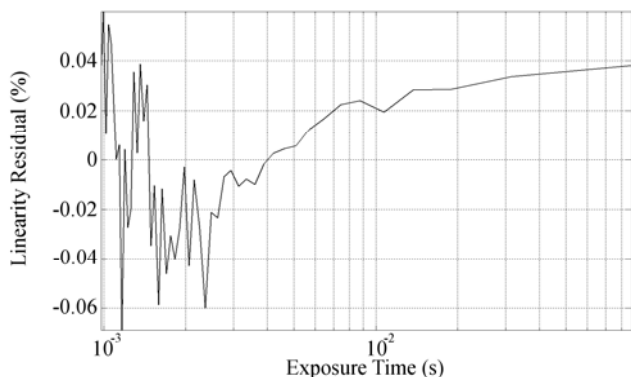


Fig. 4. Standard deviation of linearity residual plot is 302 ppm over a dynamic range of 87.1.

## V. FILTER ATTENUATION

The third method of attenuation demonstrated is the addition of a filter in the beam path. The selectable absorptive glass filter (HEBO ND 03) placed immediately behind the hyperspectral imager aperture has advantages over a thin film dielectric of lower reflected light, greater stability (because attenuations are due to bulk effects), and a simpler dependence on angle of incidence. In orbit, the filters can be calibrated directly via a succession of direct lunar radiance measurements with and without the filter in place, which, because of lunar signal levels, limits this technique to one order of magnitude of attenuation. A single filter is used to

reduce multiple reflectances or etaloning, although more than one filter is needed to span the entire shortwave spectral region. The same calibration method applies to all filters.

Unlike the other two methods of attenuation, the filter attenuation technique varies with wavelength and therefore must be calibrated using a broadband light source. A white LED with 360° output (SuperBrightLEDs RL8-W110-360) emits over the wavelength range from 450 nm to 725 nm with measured stability of 190 ppm over 87 hours. The LED is placed approximately 2 m from the instrument and the 20 mm input aperture is used throughout the entire filter calibration, as intended for orbital operations. An Atmel TH7899M CCD sensor with 16-bit resolution replaces the CMOS focal plane array to increase the measurement dynamic range for these tests. The gain linearity of this imager has been verified using the NIST calibrated trap detector. Like the previous two techniques, attenuation via filters is a relative measurement.

Fig. 5 shows the transmission ratio of one filter. Boxcar averaging and a spline fit along the wavelength direction smooth the curve. The standard deviation of the residual from this fit indicates the accuracy to which the filter can be calibrated. In the case shown in Fig. 5, the variation is 0.06% across the spectrum.

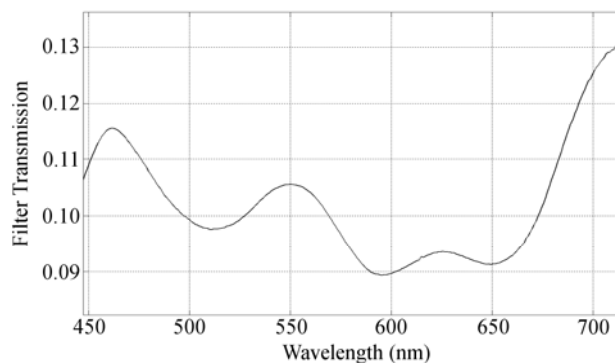


Fig. 5. Filter transmission is calibrated versus wavelength to needed accuracies.

## VI. CONCLUSIONS

The attenuation work described here promises needed measurement accuracies of a space-based radiometric calibration tied to solar irradiances relying on relative, on-orbit measurements. Assuming an uncertainty in the solar irradiance of 0.1% [1] and uncertainties of the three attenuation methods of 0.07%, 0.04%, and 0.06%, the combined measurement uncertainty for achieving the necessary five orders of magnitude attenuation is 0.14% ( $k=1$ ), meeting CLARREO requirements.

The aperture area and integration time techniques are verified in the described laboratory tests via measurements using NIST calibrated components, namely the aperture areas and the trap detector. The filter attenuation measurement is less directly tied to a NIST calibration, relying on trap detector calibrations of the FPA gain linearity. In future work, the filter verification experiment will be expanded to include a direct comparison to the trap detector.

The ranges of attenuations demonstrated collectively provide more than the required five orders of magnitude, allowing some flexibility in amount of attenuation necessary from each method and perhaps allowing further accuracy improvement. Having validated the attenuation methods individually, a system level validation utilizing the combination of all three attenuation techniques simultaneously will be demonstrated, providing a direct measurement of the full five orders of magnitude of attenuation and the associated uncertainties.

#### REFERENCES

- [1] J. Harder, G. Lawrence, J. Fontenla, G. Rottman, and T. Woods, "The Spectral Irradiance Monitor (SIM): Scientific Requirements, Instrument Design, and Operation Modes," *Solar Physics*, 230, pp. 141-176, 2007.
- [2] G. Rottman, "The SORCE Mission," *Solar Physics*, 230, pp. 7-25 2005.
- [3] M. Dinguirard and P. Slater, "Calibration of Space-Multispectral Imaging Sensors: A Review." *Remote Sens. of Environ.*, 68, pp. 194-205, 1999.
- [4] X. Xiong, N. Che, and W. Barnes, "Terra MODIS on-orbit spatial characterization and performance," *IEEE Transactions on Geoscience and Remote Sensing*, 43, 2005.
- [5] X. Xiong, H. Erivew, S. Xiong, X. Xie, J. Esposito and J. Sun, "Performance of Terra MODIS solar diffuser and solar diffuser stability monitor," *Proc. SPIE – Earth Observing Systems X*, 5882, 2005.
- [6] D. Beiso, "Overview of Hyperion On-Orbit Instrument Performance, Stability, and Artifacts," *aipr*, p. 95, 31<sup>st</sup> Applied Imagery Pattern Recognition Workshop, 2002.
- [7] R.O. Green, et al. "Imaging Spectroscopy and the Airborn Visible/Infrared Imaging Spectrometer (AVIRIS)," *Remote Sens. of Environ.* 65, pp. 227-248, 1998.
- [8] D.D.R. Kohler, W.P. Bissett, R.G. Steward, and C.O. Davis, "A New Approach for the Radiometric Calibration of Hyperspectral Imaging Systems," *Optics Express*, 12, p. 11, 2004.
- [9] R.A. Barnes and E.F. Zalewski, "Reflectance-based calibration of SeaWiFS. II. Conversion to radiance," *Appl. Opt.*, 42, 2003.
- [10] B. Guenther, et al. "MODIS Calibration: A brief review of the strategy for the at-launch calibration approach," *J. Atmos. Oceanic. Technol.*, 13, pp. 274-285, 1996.
- [11] P.M. Teillet, et al, "A generalized approach to the vicarious calibration of multiple Earth observation sensors using hyperspectral data," *Remote Sens. of Environ.*, 77, pp. 304-327, 2001.
- [12] P.M. Teillet, K.J. Thome, N. Fox, and J. Morisette, "Earth observation sensor calibration using a Global Instrumented and Automated Network of Test Sites (GIANTS)," *Proc. SPIE*, 4540, 2001b.
- [13] Committee on Earth Science and Applications from Space: A Community Assessment and Strategy for the Future, "Earth Science and Applications from Space: National Imperatives for the Next Decade and Beyond," *National Research Council*, ISBN: 0-309-66714-3, 2007.
- [14] Espejo, J., Belting, C., Drake, G., Heuerman, K., Kopp, G., Lieberman, A., Smith, P., and Vermeer, W., "A Hyperspectral Imager for High Radiometric Accuracy Earth Climate Studies," *Proc. SPIE*, Aug. 2011.
- [15] J.B. Fowler, R.D. Saunders, and A.C. Parr, "Summary of the high-accuracy aperture-area measurement capabilities at the NIST," *Metrologia* 37, 621-623, 2000.